FONT, J.M. and REDDY, R.G. Modelling of antimonate capacity in copper and nickel smelting slags. *VII International Conference on Molten Slags Fluxes and Salts,* The South African Institute of Mining and Metallurgy, 2004.

Modelling of antimonate capacity in copper and nickel smelting slags

J.M. FONT* and R.G. REDDY†

**Department of Metallurgical and Materials Engineering, Institute for Innovation in Mining and Metallurgy, Chile*

†The University of Alabama, Tuscaloosa, USA

The thermodynamic Reddy Blander (RB) model was extended for deriving antimonate capacity and antimony distribution ratio between the slag and the copper and nickel matte *a priori*. In this study, the antimonate capacities in the FeO-$FeO_{1.5}$-MgO-NiO-SiO_2, FeO-$FeO_{1.5}$-MgO-$CuO_{0.5}$-SiO_2 and FeO-$FeO_{1.5}$-MgO-NiO-CaO systems and the antimony distribution ratio for the FeO-$FeO_{1.5}$-MgO-NiO-SiO_2 slag/Ni matte, FeO-$FeO_{1.5}$-MgO-$CuO_{0.5}$-SiO_2 slag/Cu matte and FeO-$FeO_{1.5}$-MgO-NiO-CaO/Ni matte equilibrium systems were evaluated at 1523 K and 1573 K. In general, good agreement was found between the calculated RB model data and the reported experimental data for both antimonate capacity and antimony distribution ratio. The antimony distribution ratio model developed here can be extended for prediction in multi-component base metal slags and copper and nickel mattes and, thereby, may lead to develop and/or improve the efficiency of antimony removal from the base metal smelting, converting and refining processes.

Keywords: slags, copper and nickel smelting, impurity, and antimonate capacity.

Introduction

The difficulties of treating or eliminating many unwanted impurities such as As, Sb, Bi, Se, etc. in the base metal matte smelting stage have many detrimental effects. Such as on the physical properties and quality of the metal, on the environment of the surrounding areas, and on high operative cost in the overall refining process. Several researchers[1–9] have studied the behaviour of various impurities by considering thermodynamic and industry operation approaches. At present, the high oxidative smelting condition, which enhances the volatilization of impurities, is the operational trend for eliminating As and Sb from the condensed phase by collecting them after its condensation into the gas cleaning facilities of the downstream smelting-refining processes. Knowledge of the behaviour of these impurity elements in the slag phase is considered to be very important for controlling the metal refining and purification processes *a priori*.

However, much of the available information is restricted to specific experimental conditions (temperature, pO_2 and composition of the multi-component system) while for industrial data, the slag/base metal matte system data is lacking.

Recently, the authors have successfully developed a thermodynamic model for the arsenate capacity in several multi-component systems[10–11]. The arsenate capacity, which is a measure of the ability of an oxide system to hold impurity, is based on the fundamental knowledge of the chemical and solution properties of the condensed phase[12–18]. Hence, due to the very limited understanding of the antimony behaviour in the base metal slag systems, this paper presents a thermodynamic model for understanding and predicting *a priori* its behavior by determining the antimonate capacity and antimony distribution ratio between the slag and the base metal matte.

Theoretical considerations

Antimonate capacity

By considering SbO_4^{3-} as the stable species of antimony at higher temperature, and by using the same considerations of the Reddy-Blander model for the arsenate capacity derivation[10], the antimonate capacity becomes,

$$C_{SbO_4^{3-}} = \frac{\left(wt\ pct\ SbO_4^{3-}\right)}{a_{Sb}\ p_{O_2}^{5/4}} \qquad [1]$$

Where, a_{Sb} is the activity of Sb, and p_{O2} is the partial pressure of oxygen. The antimony equilibrium reaction with MO is given by:

$$\frac{3}{2}MO(1) + Sb(1) + \frac{5}{4}O_2\ (g) = M_{3/2}SbO_4(1) \qquad [2]$$

Where M is the antimonate compound forming element (Fe, Ca, etc). By combining the equilibrium constant, K_M, of reaction [2] with Equation [1], the antimonate capacity is derived for measurable quantities in Equation [3].

$$C_{SbO_4^{3-}} = \left(wt\ pct\ SbO_4^{3-}\right)\frac{K_M a_{Mo}^{3/2}}{aM_{3/2}SbO_4} \qquad [3]$$

Where, $a_{M3/2}SbO_4$ is the activity of the super cooled liquid $M_{3/2}SbO_4$.

Development of the antimonate capacity was done under the same previous considerations for deriving the arsenate capacities in the basic and acidic composition ranges[10]. Hence, the antimonate capacity for basic melts in the MO-SiO_2-$FeO_{1.5}$ system ($0 \le (X_{SiO_2} + X_{FeO_{1.5}} + \cdots) \le 0.33$) is given by Equation [4]:

$$C_{SbO_4^{3-}} = \frac{100K_M\ a_{MO}^{3/2} M_{SbO_4^{3-}}}{\left[1-2\left(X_{SiO_2} + X_{FeO_{1.5}} + ...\right)\right]} \qquad [4]$$
$$\gamma M_{3/2}SbO_4\ \overline{M}$$

Here, $\gamma M_{3/2}SbO_4$ is the Henrian activity coefficient of $M_{3/2}SbO_4$, $\overline{M}$ is the average molecular weight of the solution ($\overline{M} = M_{MO}X_{MO} + M_{SiO2}X_{SiO2} + M_{FeO1.5}X_{FeO1.5} + \cdots$). $M_{SbO_4^{3-}}$ is the molecular weight of SbO_4^{3-}, and X_i is the mole fraction of component i. While the antimonate capacity for acidic melts in the MO-SiO_2-$FeO_{1.5}$ system ($0.33 \le (X_{SiO_2} + X_{FeO_{1.5}} + \cdots) < 1$)[10,19] is given by:

$$C_{SbO_4^{3-}} = \frac{100 K_M \, a_{MO}^{3/2} M_{SbO_4^{3-}}}{\left(X_{SiO_2} + X_{FeO_{1.5}} + \ldots\right)} \frac{\phi Sb}{\overline{M}} \frac{}{a_{M_{3/2}}SbO_4} \quad [5]$$

From the Flory's approximation for monomer and polymer mixtures of silicate melts[13–18], the activity of $M_{3/2}SbO_4$ monomer units can be expressed in term of volume fraction of the Sb ion as,

$$\ln a_{M_{3/2}}SbO_4 = \ln \phi_{Sb} + \left(1 - \frac{1}{m}\right)\phi_p + \mu \phi_p^2 \quad [6]$$

Where ϕ_{Sb} and ϕ_P are the volume fractions of monomer Sb and the total polymer ($1-\phi_{Sb}$), respectively, μ is a very small constant for the weak interactions between the Sb anions and silicates, which depend on the average polymer chain length, *m*. Hence, for melts containing primarily polymers ($\phi_P \approx 1$), *m* can be obtained from the following relationship[20]:

$$\frac{1}{m} = \left(1 - a_{MO}\right)\left[\frac{1}{\left(X_{SiO_2} + X_{FeO_{1.5}} + \ldots\right)} - 2\right] \quad [7]$$

The relationship between μ and *m* for the polymer mixture is,

$$\mu = \frac{1}{4}\left(1 - \frac{1}{m}\right) \quad [8]$$

The antimonate capacity for the FeO-CaO-$FeO_{1.5}$-SiO_2 multi-component system at a constant (SiO_2+$FeO_{1.5}$) mole fraction[21] is given by,

$$\log C_{SbO_4^{3-},(Fe,Ca)O} = N_{FeO} \log C_{SbO_4^{3-},FeO} + N_{CaO} \log C_{SbO_4^{3-},CaO} + \ldots \quad [9]$$

The N_{FeO} and N_{CaO} are the electrical equivalent cationic fractions ($N_{FeO} = \frac{X_{FeO}}{X_{FeO} + X_{CaO}}$ and $N_{CaO} = \frac{X_{CaO}}{X_{FeO} + X_{CaO}}$), $C_{SbO_4^{3-},FeO}$, and $C_{SbO_4^{3-},CaO}$ are the antimonate capacities in the FeO-SiO_2 and CaO-SiO_2 binary systems at constant (SiO_2+$FeO_{1.5}$ +···) mole fractions, and $C_{AsO_4^{3-},(Fe,Ca)O}$ is the antimonate capacity of the FeO-CaO-$FeO_{1.5}$-SiO_2 system. Hence, for a given composition ($0 \le X_{SiO_2} + X_{FeO_{1.5}} + \cdots < 1$) and temperature, the antimonate capacity of binary and multi-components systems can be predicted by using Equations [4], [5] and [9].

The equilibrium constant for reaction [2] at 1523 K and 1573 K is presented in Table I for different MO-SiO_2 binary systems. It is important to note that due to the lack of liquid data for $Ca_{3/2}SbO_4$, $Mg_{3/2}SbO_4$, $Ni_{3/2}SbO_4$ and $Cu_{3/2}SbO_4$ system, the available solid data of $M_{3/2}SbO_4$[21] was used in calculating the Gibbs energy for reaction [2]. Nevertheless, it is expected that when the liquid data is used, the antimonate capacity will be in some extent larger than those estimated with the solid data.

Antimony distribution ratio

The antimony experimental data were reported mainly in the form of distribution ratio between the slag and the base metal matte (Ni, Cu), defined as $L_{Sb}^{s/m} = \frac{(\text{wt pct Sb in slag})}{\{\text{wt pct Sb in base metal matte}\}}$. Hence, similar to the previously derived $L_{As}^{s/m}$[10–11], an expression for the distribution ratio and the antimonate capacity model was derived for the *a priori* $L_{Sb}^{s/m}$, as given in Equation [10].

$$L_{Sb}^{s/m} = \frac{C_{SbO_4^{3-}} \, \gamma Sb \, p_{O_2}^{5/4}}{M_{SbO_4^{3-}} \{n_T\}} \quad [10]$$

Where γ_{Sb} and $\{n_T\}$ are the antimony activity coefficient and the total number of moles per 100 g of base metal matte, respectively.

Results and discussion

Effect of matte species on antimonate capacities and antimony distribution ratio

The RB antimonate capacities were calculated for each of the slag composition data reported experimentally in the Ni and Cu matte in equilibrium with quantities of NiO and $CuO_{0.5}$ in the FeO-$FeO_{1.5}$-MgO-SiO_2 base slag at 1573 K and pSO_2 of 0.1, respectively[2,5]. The experimental antimonate capacities were derived by using Equation [9] and the reported data of $L_{Sb}^{s/m}$ for the Ni or Cu matte[2,5]. The data of γ_{Sb} for the Ni[2] or Cu matte[4], the a_{MO} in the MO-SiO_2 binary system[23], and the experimental pO_2 and $\{n_T\}$ were also used in the calculations. Figure 1 shows the experimental and RB antimonate capacities for the FeO-$FeO_{1.5}$-MgO-NiO-SiO_2 system (1-a) and the experimental and RB antimony distribution ratios between the Ni matte and the FeO-$FeO_{1.5}$-MgO-NiO-SiO_2 slag (1-b).

Figure 2 shows the experimental and RB antimonate capacities for the FeO-$FeO_{1.5}$-MgO-$CuO_{0.5}$-SiO_2 system (2-a), and the experimental and RB antimony distribution ratio between the Cu matte and the FeO-$FeO_{1.5}$-MgO-$CuO_{0.5}$-SiO_2 slag system (2-b).

It is clearly noted in Figures 1 and 2 that there is good agreement between the calculated RB model and the experimental data for the antimonate capacities and antimony distribution ratios at 1573 K and pSO_2 of 0.1. It is important to highlight that these good agreements may be ascribable to the accurate composition of the slag, which includes the dissolved quantities of NiO or $CuO_{0.5}$ that affect the composition of X_{MO} in the slag and the a_{MO} in the RB antimonate calculations. This is especially true at high matte grade where the dissolution of Ni or Cu into the slag is considerably high. Moreover, the slight differences between the RB model calculated data and the experimental ones may be due to the uncertainties of the experimental $L_{Sb}^{s/m}$ values, and the Gibbs energy value estimated from the

Table I
Equilibrium Constants for Antimonate Forming Reactions[22–23]

M[(1)]	Log K_M (reaction 2)	
	1523 K	1573 K
Fe[(2)]	11.0	10.4
Ca	10.3	-
Mg	10.2	9.6
Cu	-4.7	-6.0
Ni[(2)]	3.4	3.1

[(1)]Solid state [(2)]Estimated for liquid

solid data. Table II shows the experimental and calculated antimonate capacities and antimony distribution ratio at 1573 K and 1523 K.

Effect of slag composition and temperature on antimonate capacities and antimony distribution ratio

As shown in Figures 1 and 2, the good agreements between the model calculated RB and the experimental data were achieved for multi-component systems with high acidic components. However, for basic systems like multi-component systems with $X_{SiO_2} \approx 0$, it is important to evaluate the antimonate capacity by the RB model. Thus, considering the slag composition obtained from the reported antimony distribution ratio data between the FeO-$FeO_{1.5}$-MgO-NiO-CaO slag ($X_{SiO_2} = 0$) and Ni matte at 1523 K and pSO_2 of 0.1[7], the RB antimonate capacity was calculated using Equation [4]. The results are presented in Table II and Figure 3(a). The experimentally derived antimonate capacity data are also included in the Figure. These were derived by considering Equation [10] for the reported data of $L_{Sb}^{s/m}$ γ_{Sb}, pO_2, $\{n_T\}$, and a_{MO}[2,7,23], while Figure 3(b) shows the experimental and the derived RB antimony distribution ratio. In general, in Figure 3, a good agreement is noted between the experimental and the RB calculated antimonate capacity and $L_{Sb}^{s/m}$ data.

Moreover, when the temperature effect is taken into account, a good agreement is noted between the calculated RB antimonate capacity and $L_{Sb}^{s/m}$ with those experimental ones (see Figures 1–3). This effect is ascribable mainly to the K_{MO} values used in Equations [4] and [5].

Conclusions

The thermodynamic Reddy Blander model was extended for *a priori* predictions of antimonate capacity and antimony distribution ratio between the slag and the base metal mattes. The derived RB model was used for evaluating several multi-component slags and base metal mattes (Ni and Cu) at different pSO_2 (0.1, 0.5 and 1) and temperatures (1523 K and 1573 K). A good agreement was clearly found between the calculated RB model and the reported experimental data for both antimonate capacities in the FeO-$FeO_{1.5}$-MgO-NiO-SiO_2, FeO-$FeO_{1.5}$-MgO-$CuO_{0.5}$-SiO_2, and FeO-$FeO_{1.5}$-MgO-NiO-CaO systems, and antimony distribution ratio between the FeO-$FeO_{1.5}$-MgO-NiO-SiO_2 slag/Ni matte, FeO-$FeO_{1.5}$-MgO-$CuO_{0.5}$-SiO_2 slag/Cu matte, and FeO-$FeO_{1.5}$-MgO-NiO-CaO/Ni matte. The use of this model for *a priori* prediction of other impurity capacities, such as Bi, Cr, Se, and Te in the non-ferrous smelting slags and mattes is very feasible. Such predictions will be very useful in understanding the behaviour of impurities, and therefore new developments and improvements for *a priori* impurity control in the non-ferrous smelting processes may be achieved.

Acknowledgments

The authors are pleased to acknowledge the financial support for this research from American Cast Iron Pipe Company (ACIPCO), and the University of Alabama Pyrometallurgy Funds.

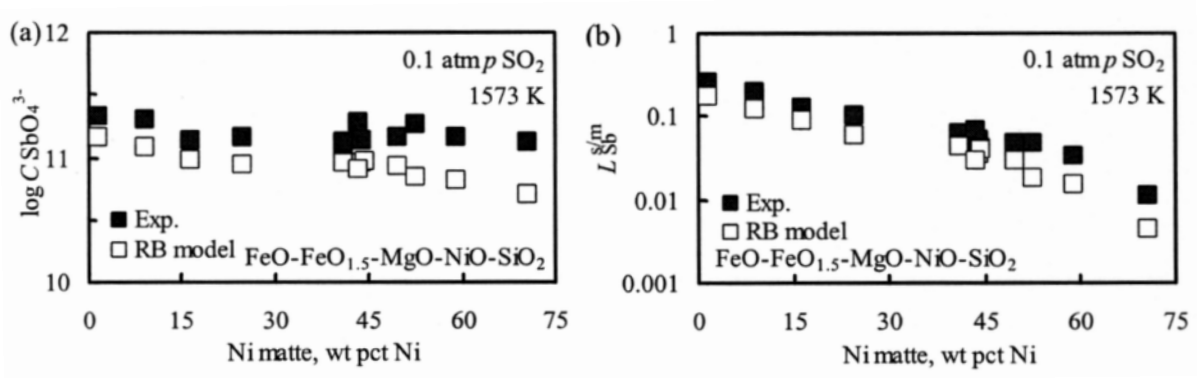

Figure 1. Antimonate capacity for the FeO-$FeO_{1.5}$-MgO-NiO-SiO_2 multi-component system (a), and antimony distribution ratio between the FeO-$FeO_{1.5}$-MgO-NiO-SiO_2 slag and Ni matte at 1573 K and pSO_2 of 0.1 (b)

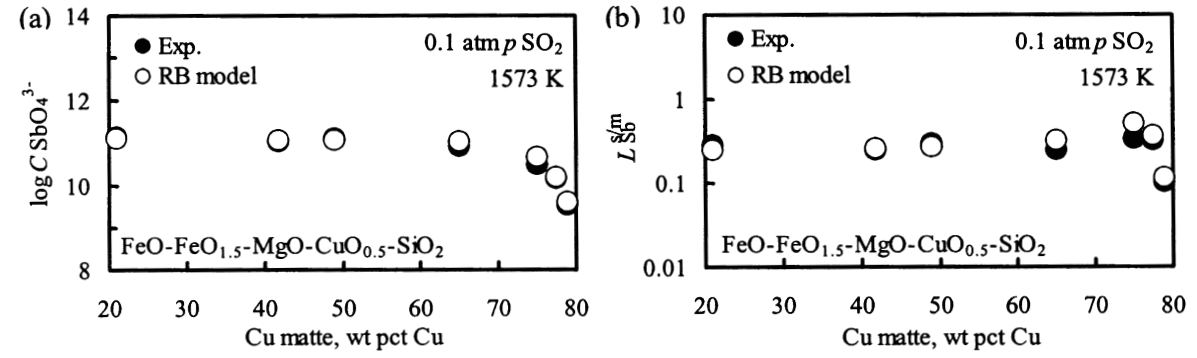

Figure 2. Antimonate capacity for the FeO-$FeO_{1.5}$-MgO-$CuO_{0.5}$-SiO_2 multi-component system (a), and antimony distribution ratio between the FeO-$FeO_{1.5}$-MgO-$CuO_{0.5}$-SiO_2 slag and Cu matte at 1573 K and pSO_2 of 0.1 (b)

Table II
Experimental and calculated antimonate capacities and antimony distribution ratio at 1573 and 1523 K[2–7]

					Matte, wt pct		Slag, molar pct							$\log C_{SbO_4}$		$L_{Sb}^{s/m}$	
Temp. K	pSO_2	pO_2	$\{n_T\}$	γ_{Sb}	Ni	Cu	FeO	$FeO_{1.5}$	NiO	$CuO_{0.5}$	MgO	SiO_2	CaO	RB model	Exp.	RB model	Exp.
1573	0.1	8.8E-09	1.21	1.02	44.0		48.2	4.3	0.33		9.5	37.7		10.96	11.13	0.04	0.05
1573	0.1	9.2E-09	1.20	1.20	41.1		48.5	3.5	0.35		9.9	37.7		10.97	11.01	0.04	0.05
1573	0.1	9.0E-09	1.20	1.21	41.0		48.0	4.7	0.33		9.3	37.7		10.96	11.12	0.04	0.06
1573	0.1	1.0E-08	1.21	0.72	49.6		48.1	2.7	0.36		9.7	39.1		10.93	11.16	0.03	0.05
1573	0.1	1.5E-08	1.22	0.33	58.9		46.0	3.8	0.73		10.4	39.1		10.81	11.17	0.02	0.03
1573	0.1	9.8E-09	1.21	1.00	44.4		48.4	3.9	0.33		9.3	38.1		10.96	10.97	0.04	0.04
1573	0.1	8.1E-09	1.20	1.06	43.4		47.1	3.7	0.32		10.6	38.3		10.90	11.28	0.03	0.07
1573	0.1	4.9E-09	1.17	5.31	9.0		51.3	2.3	0.16		7.6	38.6		11.09	11.30	0.12	0.20
1573	0.1	4.5E-09	1.17	7.16	1.5		52.0	3.0	0.01		8.8	36.2		11.16	11.33	0.17	0.26
1573	0.1	2.4E-08	1.24	0.07	70.6		44.7	5.2	1.25		7.9	41.0		10.71	11.12	0.00	0.01
1573	0.1	6.1E-09	1.18	3.83	16.4		48.9	3.4	0.27		9.1	38.4		10.98	11.13	0.09	0.13
1573	0.1	6.5E-09	1.18	2.61	24.7		47.7	3.8	0.24		10.3	38.0		10.94	11.16	0.06	0.10
1573	0.1	1.0E-08	1.22	0.59	52.5		46.4	3.8	0.60		9.7	39.6		10.84	11.26	0.02	0.05
1573	0.1	5.8E-09	1.18	8.68		21.0	50.8	8.0		0.45	8.2	32.5		11.08	11.14	0.24	0.28
1573	0.1	6.1E-09	1.20	9.20		42.0	50.7	8.1		0.52	8.2	32.4		11.06	11.04	0.26	0.24
1573	0.1	6.5E-09	1.21	8.75		49.0	50.6	8.3		0.49	8.2	32.5		11.06	11.11	0.26	0.29
1573	0.1	9.4E-09	1.24	7.96		65.0	49.8	9.1		0.59	8.2	32.4		11.00	10.89	0.32	0.25
1573	0.1	4.1E-08	1.25	4.59		75.0	45.6	13.2		1.54	8.3	31.4		10.65	10.46	0.51	0.33
1573	0.1	1.1E-07	1.25	2.69		77.5	41.8	17.0		3.25	8.3	29.7		10.19	10.14	0.36	0.32
1573	0.1	2.5E-07	1.26	1.25		79.0	37.8	21.1		6.23	8.4	26.4		9.57	9.52	0.11	0.10
1523	0.1	1.1E-08	1.24	0.07	69.5		30.3	31.4	3.66		5.2		29.4	12.22	12.71	0.06	0.18
1523	0.1	9.2E-09	1.24	0.10	67.7		32.5	27.4	4.12		6.9		29.1	12.34	12.71	0.08	0.19
1523	0.1	6.9E-09	1.23	0.15	65.0		45.1	18.7	3.23		4.3		28.7	12.71	12.81	0.21	0.26
1523	0.1	5.4E-09	1.23	0.23	61.6		50.3	12.7	3.71		4.0		29.3	12.83	12.83	0.32	0.32
1523	0.1	5.7E-09	1.23	0.19	63.3		47.2	16.0	3.95		5.2		27.7	12.73	12.90	0.22	0.33
1523	0.1	4.6E-09	1.23	0.31	59.1		59.2	8.6	3.01		3.1		26.1	13.00	12.73	0.52	0.28
1523	0.1	3.6E-09	1.22	0.52	53.8		58.0	7.6	4.30		3.6		26.6	12.93	12.66	0.54	0.29

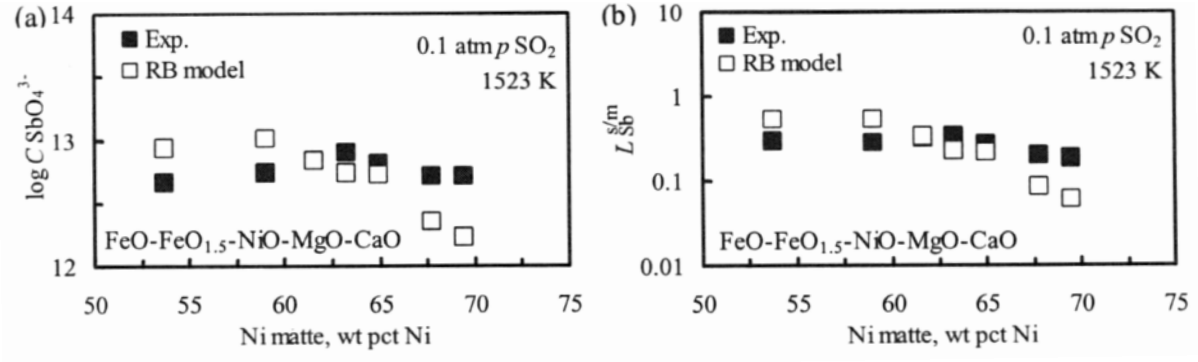

Figure 3. Antimonate capacity for the $FeO\text{-}FeO_{1.5}\text{-}NiO\text{-}MgO\text{-}CaO$ multi-component system (a), and antimony distribution ratio between the $FeO\text{-}FeO_{1.5}\text{-}NiO\text{-}MgO\text{-}CaO$ slag and Ni matte at 1523 K and pSO_2 of 0.1 (b)

References

1. REDDY, R.G. Recovery of Pollution Causing Elements from Copper Slags, *Minor Elements 2000: Processing and Environmental Aspects of As, Sb, Se, Te, and Te,* Young, C. (ed.) Littleton, CO: SME, 2000, pp. 239–249.
2. FONT, J.M., HINO, M., and ITAGAKI, K. Minor Elements Distribution between Iron-Silicate Base Slag and Ni_3S_2-FeS Matte under High Partial Pressures of SO_2. *Mater. Trans. JIM*, vol. 39, 1998. pp. 834–840.
3. FONT, J.M., HINO, M., and ITAGAKI, K. Thermodynamic Evaluation of Distribution Behavior of VA Elements in Nickel Matte Smelting. *Metal. Rev. of the MMIJ*, vol. 15 no. 2, 1998. pp. 202–220.
4. ITAGAKI, K. and YAZAWA, A. Thermodynamic Evaluation of Distribution Behaviour of Arsenic, Antimony and Bismuth in Copper Smelting. *Advances in Sulfides Smelting Symposium*, Sohn, H.Y., George, D.B. and Zunkel, A.D. Warrendale, P.A. (eds.). The Metallurgical Society of AIME, 1983. pp. 119–142.
5. ROGHANI, G., TAKEDA, Y., and ITAGAKI, K. Phase Equilibrium and Minor Element Distribution between FeO_X-SiO_2-MgO-Based Slag and Cu_2S-FeS Matte at 1573 K under High Partial Pressures of SO_2. *Metall. Trans. B*, vol. 31, 2000. pp. 705–712.
6. FONT J.M., HINO M., and ITAGAKI K. Phase Equilibrium Minor and Elements Distribution between Iron-Silicate Base Slag and Nickel-Copper-Iron Matte at 1573 K under High Partial Pressures of SO2. *Mater. Trans. JIM*, vol. 40, 1999. pp. 20–26.
7. FONT J.M., HINO M., and ITAGAKI K. Phase Equilibrium and Minor-Element Distribution between Ni_3S_2-FeS Matte and Calcium Ferrite slag under High Partial Pressures of SO2. *Metall. Trans. B*, vol. 31, 2000. pp. 1231–1239.
8. ROGHANI G., HINO M., and ITAGAKI K. Phase Equilibrium and Minor Elements Distribution between SiO_2-CaO-FeO_X-MgO Slag and Copper Matte at 1573 K under High Partial Pressures of SO_2. *Mater. Trans. JIM*, vol. 38, 1997. pp. 707–713.
9. NIKOLOV S., JALKANEN H., and KYTO M. Distribution of some Impurity Elements between High Grade Copper Matte and Calcium Ferrite Slag.

4th Inter. Conf. on Molten Slags and Fluxes, Sendai, Japan, ISIJ, 1992. pp. 560–565.

10. REDDY R.G. and FONT J.M. Arsenate Capacities of Copper Smelting Slag. *Metall. Trans. B*, 2003. In press.

11. FONT J.M. and REDDY R.G. Modeling of Arsenic Distribution between Slags and Copper Mattes or Liquid Copper. *Proceeding of the Yazawa International Symposium*. Sohn H.Y., Itagaki K., Yamauchi C. and Kongoli F. (eds.). TMS, Warrendale, 2003. pp. 991–1003.

12. FINCHAM C.J.B. and RICHARDSON F.D. The Behaviour of Sulphur in Silicate and Aluminate *Melts. Proc. Royal. Soc. of London*, vol. 223A, 1954. pp. 40–62.

13. REDDY R.G. and BLANDER M. Modeling of Sulfide Capacities of Silicate Melts. *Metall. Trans. B,* vol. 18, 1987. pp. 591–596.

14. REDDY R.G. and BLANDER M. Sulfide Capacities of $MnO\text{-}SiO_2$ Slags. *Metall. Trans. B,* vol. 20, 1989. pp. 137–140.

15. REDDY R.G., HU H., and BLANDER M. Sulfide Capacities of Silicate Slags. *4th Inter. Conf. on Molten Slags and Fluxes*, Sendai, Japan, ISIJ, 1992. pp. 144–148.

16. CHEN B., REDDY R.G., and BLANDER M. Sulfide Capacities of $CaO\text{-}FeO\text{-}SiO_2$ Slags. *3rd International Conference on Molten Slags and Fluxes*, Glasgow, Scotland, The Institute of Metals, 1988. pp. 270–272.

17. REDDY R.G. and ZHAO W. Sulfide Capacities of $Na_2O\text{-}SiO_2$ Melts. *Metall. Trans. B,* vol. 32, 1995. pp. 925–928.

18. PELTON A.D., ERIKSSON G., and ROMERO-SERRANO A. Calculation of Sulfide Capacities of Multi-component Slags. *Metall. Trans. B*, vol. 24, 1993. pp. 817–825.

19. HILDEBRAND J.H. and SCOTT R.L. The Solubility of Non-Electrolytes. New York: Reinhold Publishing Corporation, 1950. p. 347.

20. MASSON C.R., SMITH I.B., and WHITEWAY S.G. Activities and Ionic Distributions in Liquid Silicates: Application of Polymer Theory. *Can. J. Chem*., vol. 48 1970. pp. 1456–1464.

21. FLOOD H. and GRJOTHEIM K. Thermodynamic Calculation of Slag Equilibria. *JISI*, vol. 171, 1952. pp. 64–70.

22. HSC Chemistry software, A. Roine, ver. 4.1, Outokumpu Research Oy, Pori, Finland.

23. FactSage™ 5.0 software, Thermfact Ltd. (Montreal) and GTT-Technologies, Aachen. 2001.